European Journal of Medicinal Chemistry 276 (2024) 116676

Contents lists available at ScienceDirect

European Journal of Medicinal Chemistry

journal homepage: www.elsevier.com/locate/ejmech

Research paper

Biological and structural investigation of tetrahydro-β-carboline-based selective HDAC6 inhibitors with improved stability

Simon Scheuerer [a], Lucia Motlova [b], Linda Schäker-Hübner [c], Andreas Sellmer [a], Felix Feller [c], Fabian J. Ertl [d], Pierre Koch [d,1], Finn K. Hansen [c,1], Cyril Barinka [b,1], Siavosh Mahboobi [a,*,1]

[a] Institute of Pharmacy, Department of Pharmaceutical/Medicinal Chemistry I, University of Regensburg, 93040, Regensburg, Germany
[b] Institute of Biotechnology of the Czech Academy of Sciences, BIOCEV, Prumyslova 595, 252 50, Vestec, Czech Republic
[c] Pharmaceutical Institute, Department of Pharmaceutical and Cell Biological Chemistry, University of Bonn, 53121, Bonn, Germany
[d] Institute of Pharmacy, Department of Pharmaceutical/Medicinal Chemistry II, University of Regensburg, 93040, Regensburg, Germany

ARTICLE INFO

Keywords:
Histone deacetylase inhibitors
HDAC selectivity
Enantiomers
Tetrahydro-β-carboline
Phenylhydroxamate
Chemical structure

ABSTRACT

Our previously reported HDAC6 inhibitor (HDAC6i) Marbostat-100 (**4**) has provided many arguments for further clinical evaluation. By the substitution of the acidic hydrogen of **4** for different carbon residues, we were able to generate an all-carbon stereocenter, which significantly improves the hydrolytic stability of the inhibitor. Further asymmetric synthesis has shown that the (*S*)-configured inhibitors preferentially bind to HDAC6. This led to the highly selective and potent methyl-substituted derivative *S*-**29b**, which elicited a long-lasting tubulin hyperacetylation in MV4-11 cells. Finally, a crystal structure of the HDAC6/*S*-**29b** complex provided mechanistic explanation for the high potency and stereoselectivity of synthesized compound series.

1. Introduction

Posttranslational modifications like methylation, phosphorylation, and acetylation of the chromatin play a major role in many cellular and molecular processes. [1] The packing of the chromatin is directly related to the degree of acetylation of the histones, constituting the primary protein components of this complex, thus regulating the accessibly of the DNA for gene expression. [2–4] In addition to histones, acetylation and deacetylation also occur on non-histone proteins located in the nucleus and the cytoplasm. [5–7] Two different types of enzymes are responsible for the acetylation status of the lysine side chains of proteins: Histone deacetylases (HDACs) remove the acetyl groups, whereas histone acetyltransferases (HATs) attach those acetyl groups. [8] So far 18 mammal HDACs isoenzymes – divided into four classes – have been identified. With exception of the NAD^+ dependent sirtuins of class III, all other HDACs (class I, IIa, IIb, IV) are zinc dependent. [9] In contrast to all other members of the HDAC family HDAC6 contains two catalytically active deacetylase domains (CD1 and CD2) [10]. It is found primarily in the cytoplasm due to its nuclear export signal (NES) targeting non-histone proteins, such as α-tubulin, HSP90, cortactin and peroxiredoxin. [5,11–15].

Targeting a large variety of proteins in the cytoplasm, any malfunction of acetylation influences cellular homeostasis and can lead to several diseases [16]. HDAC6 inhibitors have shown to be a promising tool against cancer [17], neurodegenerative [18,19] and inflammatory diseases [20]. So far four HDAC inhibitors (HDACis) are approved by the FDA, including Vorinostat (**1**) and Panobinostat (**2**) (Fig. 1A) for the treatment of T cell lymphomas and multiple myeloma [21]. Unfortunately, these and other first generation – so called pan-HDAC inhibitors – lack isoform selectivity which leads to side effects like fatigue, thrombocytopenia and diarrhea [22–24]. In selectively inhibiting HDAC6 these drawbacks could be addressed [25]. In fact, HDAC6 knock out mice possessing hyperacetylated tubulin in most tissues proved to be viable and develop normally [26]. Consequently, the demand for isoform specific HDACis has increased. Currently under clinicals trials, Ricolinostat (**3**) (Fig. 1A) represents a selective HDAC6 inhibitor for the treatment of multiple myeloma [27].

The classical pharmacophore model of HDAC inhibitors consists of a zinc-binding group (ZBG) coordinating the zinc ion in the active site, a linker spanning the hydrophobic HDAC channel and a capping group interacting with amino acids of the rim region (Fig. 1A) [28,29]. A broad range of selective HDAC6 inhibitors has been synthesized, using

* Corresponding author.
E-mail address: Siavosh.mahboobi@chemie.uni-regensburg.de (S. Mahboobi).
[1] These senior authors contributed equally.

https://doi.org/10.1016/j.ejmech.2024.116676
Received 3 April 2024; Received in revised form 30 June 2024; Accepted 10 July 2024
Available online 14 July 2024

different approaches to enhance isoform selectivity by modification of the three functional motifs, predominantly focusing on the capping group. The linker is quite conserved and comprises either a long flexible aliphatic chain or bulky and rigid aromatic moiety.[9] Hydroxamic acids are widely used ZBGs yet, in recent years other ZBGs, especially mercaptoacetamides and fluoroalkyl-oxadiazoles, have been used for selective HDAC6 inhibition trying to avoid the potential side effects of hydroxamic acids [30–35].

The x-ray crystallography structure of HDAC6 reported by Hai et al. highlights essential differences of the two catalytic domains [10]. HDAC6 co-crystallization with different inhibitors gave fundamental insight into the binding mode, which pushed forward the structural based drug design. We have recently reported the highly selective and potent HDAC6 inhibitor **4** [29] which is based on the lead structure Tubastatin A (TubA) (**5**), containing a tetrahydrocarboline cap (Fig. 1B) [36]. Additionally, the crystal structure of zHDAC6-CD2 in complex with TubA provided detailed insights concerning the binding mode and interactions with amino acids of the HDAC6 binding pocket [37].

To further investigate the structure-activity relationship (SAR), we introduced different carbon residues at the chiral center to substitute the acidic proton in **4**. For selected key compounds, the (*R*)- and (*S*)-enantiomers were synthesized in addition to the racemates to elucidate the stereochemical influence in more detail (Fig. 1B). With regard to the acidic proton, a potential improvement of the racemic and the hydrolytic stability was also of interest. To go one step further, we connected a phenyl linker containing the hydroxamic acid to the chiral center directly, leaving the indole nitrogen vacant for possible substitutions (Fig. 1C). Finally, we were able to solve a crystal structure of our compound *S*-**29b** in complex with zHDAC6-CD2 to gain detailed insight into the binding mode.

2. Results and discussion

In order to extend the SAR, various residues were introduced at the chiral center of **4**. Key step for the synthesis of the racemic compounds was a Friedel-Crafts alkylation of indoles **11**–**13** with electron-deficient

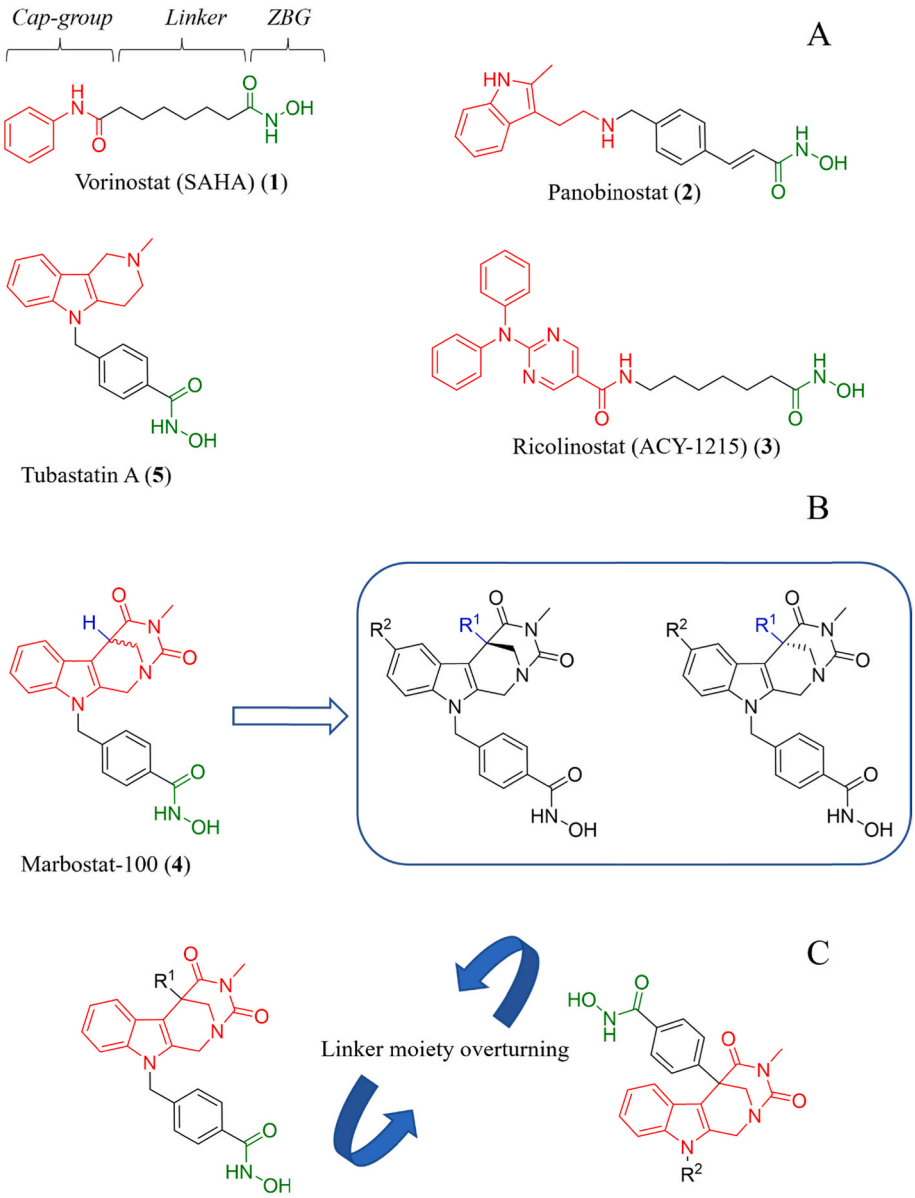

Fig. 1. (**A**) Schematic representation of HDAC6 inhibitors including the lead structure Tubastatin A. General design of HDACis containing a capping group (colored red), linker, and ZBG (colored green) (left). (**B**) General structures of the compounds investigated. Enantioselective modification at the chiral center by different residues (colored blue) of the inhibitor **4** containing a dihydrouracil moiety. (**C**) Linker moiety overturning.

Michael acceptors **10** (Scheme 1) to produce indolic β-nitroesters **14a-h**, containing an all-carbon quaternary stereocenter [38]. Starting from α-keto ester **8**, Henry reaction using nitro methane and subsequent dehydration of **9** led to the desired nitro olefines **10** [39]. To obtain selected (*R*)- and (*S*)-enantiomers asymmetric synthesis of the intermediate **14** was required (Scheme 1). The corresponding (*S*)-enatiomers ***S*-10a,b,f** were accessible via the established Iridium catalyst **15** [40] (Table 1) and the (*R*)-configurated ***R*-10b** via chiral phosphoric acid **16** [41] (Scheme 2).

Xu *et al.* [40] have developed a highly enantioselective catalyst for the Friedel-Crafts alkylation of indoles with β,β-disubstituted nitroalkenes. To obtain the ligands for the synthesis of iridium catalyst **15** minor changes were needed within the described procedures [40,42]. Since the substrates used in this work were in parts different to the literature, adjustments had to be made: The selection of different solvents, temperatures and catalyst loadings had a great impact on the yield and enantioselectivity of the reaction. A detailed overview is given in Table 1. Application of the proposed synthetic conditions led to 93–94 % enantioselectivity and yield of 99 % with indole (entry 10) and 5-methoxyindole (entry 11) as starting materials. However, with 5-benzyloxyindole enantiomeric excess (ee) and yield decreased significantly with the need of a longer reaction time. In contrast to the unsubstituted indole and 5-methoxyindole, 5-benzyloxyindole with its bulky residue on the 5-position showed extremely poor solubility in toluene. Raising the reaction temperature to overcome the solubility issues led to improved yields but decreased the ee. Screening other solvents with good solubility showed that a 1:1 mixture of toluene with either $CHCl_3$ or CH_2Cl_2 successfully improved the ee up to 90 %. Catalyst loading of 0.4 mol % was required, higher concentrations did not improve the ee significantly. Exchange of the phenyl-for a methyl-group at the alkene required further adaption of the reaction conditions. A temperature of −20 °C, CH_2Cl_2 as solvent and a reaction time of 42 h yielded the methyl derivative (entry 12) with 95 % enantiomeric excess and a yield of 79 %. A comparison of the differently substituted indoles and alkenes indicates that the size of the residue could influence the enantiomeric excess. With only one sterically demanding moiety (entry 10,11,12) enantiomeric excesses of 92–95 % are achieved, compared to reaction of 5-benzyloxyindole and phenyl nitroalkene with 90 % ee (entry 3). To access the corresponding (*R*)-enantiomer ***R*-14b**, containing the methyl residue at the all-carbon stereocenter, chiral phosphoric acid **16** was used as the catalyst (Scheme 2) [41]. The reaction of 5-benzyloxyindole with methyl **10b** gave rise to the desired ***R*-14b** with an enantiomeric excess of 82 %.

After the successful synthesis of the desired Friedel-Crafts adducts

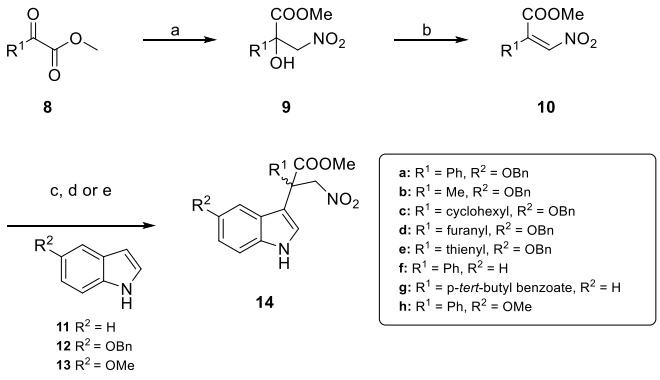

Scheme 1. Introduction of different residues at the capping group. Reagents and conditions: a) CH_3NO_2, NEt_3, rt., 24 h, 63–99 %; b) $SOCl_2$, NEt_3, rt., 1–3 h, 22–85 %; c) for racemate: indole, calcium(II) bis(trifluoromethanesulfonimide) ($Ca(NTf_2)_2$), rt., 24 h, 29–99 %; d) for (*S*)-configuration: indole, chiral catalyst Λ-(*R*,*R*)-Ir4, rt., darkness, 36 h, 79–99 %; for (*R*)-configuration: indole, (11bR)-4-hydroxy-2,6-bis(2,4,6-triisopropylphenyl)dinaphtho[2,1-d:1′,2′-f][1,3,2]dioxaphosphepine 4-oxide (**16**), powdered MS 5 Å, rt, 3 d, 84 %.

14, the final assembly of the ring structure and hydroxamic acid was carried out according to the previously reported synthesis, summarized in Scheme 3 and Scheme 4 [29].

Since the chiral center at C-5 of **4** contains an acidic proton, the introduction of the new residues could potentially influence the stability of the compounds. As described in the literature, deprotonation of structurally close hydantoins leads to racemization [43] and hydrolysis [44], consequently **4** may also be affected. The racemization of hydantoins, being homologues of dihydrouracils, is documented to a great extent in the literature under various conditions following general base catalysis [45–48]. Even at mild basic conditions at the physiological pH 7.4 in a phosphate buffer system racemization is observed, mediated by the divalent phosphate ion [49,50]. The proton exchange proceeds via an enolate intermediate [51].

Contrary to hydantoins, little references are found on the stability of dihydrouracils. The study of monosubstituted 5-methyl-dihydrouracil, containing an acidic proton adjacent to a carbonyl group, shows racemization [51,52]. However, if the stereocenter is located at C-6, as in 6-benzyldihydrouracil, for example, racemization does not occur due to the absence of an adjacent carbonyl group [52].

To prevent any impact of its acidic nature, the hydrogen of Marbostsat-100 at the C-5 was exchanged by a carbon containing residue. As reported, the exchange of the proton at the stereocenter of thalidomide by a methyl group leads to the stable non-racemizing methylthalidomide [53,54].

In view of the well-known racemization of structurally close molecules, racemization of **4** seemed plausible. Due to chiral resolution, the precursor carboxylic acid of **4** (**Carb-Marb**) was used as a model for the investigation. However, no racemization was observed in phosphate buffer (pH = 7.4, 50 nM) for **Carb-Marb** at 37 °C after 24 h (Fig. 2; Fig. 3C). The dihydrouracil moiety of **Carb-Marb** however, hydrolyzed (**HP-1**) at these mild conditions, expected only at higher pH values (Fig. 3A) [51]. Hydantoins and dihydrouracils showed no hydrolysis under similar conditions [51,55]. After 3 days even decarboxylation of the hydrolysis product (**HP-2**) was observed (Fig. 3A; Fig. 2). As expected, the exchange of the hydrogen at the chiral center for a carbon moiety, generating an all carbon stereocenter, prevented racemization. More importantly, the absence of an acidic proton at the stereocenter improved the stability significantly. Under the same conditions the 5-phenyl derivative ***S*-25f** showed hardly any hydrolysis after 3 days (Fig. 3B). Similar results were obtained for the 5-methyl derivatives ***S*-25b** and ***S*-29b** in PBS buffer (Fig. S2). Since the acidic proton is also replaced by a carbon residue in all other compounds (**25a-e**), improved stability can also be expected for these substances. Further, the stability of ***S*-25b** and ***S*-29b** was assessed in human plasma, exhibiting high plasma stability (Table 2).

The synthesized compounds **29a-f** were then tested *in vitro* for their inhibitory effect against HDAC isoforms. Special emphasis was placed on the influence of the corresponding enantiomers. For the validation of potency and selectivity of HDACs 1, 2, 3, 6 and 8, the inhibition was measured in assays using recombinant purified human HDAC proteins.

The determined K_i values are listed in Table 3. All tested compounds inhibit HDAC6 preferentially with K_i values ranging from 0.31 to 1.64 nM. The influence of the different residues at the chiral center has no major impact on the affinity of the tested compounds. A comparison of the different enantiomers respectively racemates tends to a moderately increased activity of the (*S*)-enantiomers, with an eudismic ratio of 0.4 for the methyl derivative (entries 6–8). All compounds selectively address HDAC6 over HDAC1-3 ($K_i > 50$ nM) and HDAC8 ($K_i > 600$ nM). Connecting the hydroxamic acid via the phenyl linker directly to the stereocenter led to a decrease of the affinity overall (see Table 4). The compounds K_i containing the intact dihydrouracil moiety range from 64 to 247 nM, the lowest resulting from the unsubstituted indole nitrogen **29g**. A lower K_i of 17 nM was obtained from **29j**, lacking the dihydrouracil ring at all, with only a methyl ester at the chiral center.

To investigate whether the results gained in the *in vitro* HDAC

Table 1
Enantioselective synthesis of differently substituted nitroalkenes[a].

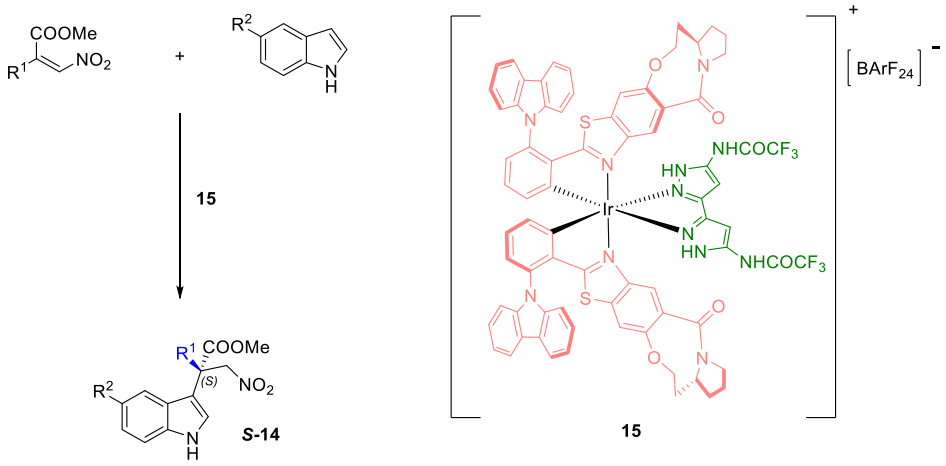

entry	solvent	(mol %)[b]	R_1	R_2	temp. (°C)	t (h)	yield[c] (%)	ee[d] (%)
1	toluene	0.2	Ph	OBn	40	72	71	57
2	toluene	0.1	Ph	OBn	rt.	120	54	66
3	toluene/CH_2Cl_2 1:1	0.4	Ph	OBn	rt.	20	97	90
4	toluene/$CHCl_3$ 1:1	0.4	Ph	OBn	rt.	20	98	90
5	dioxane	0.4	Ph	OBn	rt.	20	88	86
6	tetrahydrofuran	0.4	Ph	OBn	rt.	20	44	78
7	toluene/CH_2Cl_2 1:1	0.3	Ph	OBn	rt.	38	96	85
8	toluene/CH_2Cl_2 1:1	0.4	Ph	OBn	rt.	38	97	90
9	toluene/CH_2Cl_2 1:1	0.6	Ph	OBn	rt.	38	97	92
10	toluene	0.3	Ph	H	rt.	20	99	92[e]
11	toluene	0.4	Ph	OMe	rt.	24	99	94
12	CH_2Cl_2	0.4	Me	OBn	−20	42	79	95[f]

[a] $BArF_{24}$ = tetrakis[3,5-di(trifluoromethyl)phenyl]borate.
[b] Catalyst loadings provided in mol %.
[c] Isolated yield.
[d] Determined by chiral HPLC.
[e] Determined from *S*-**19f**.
[f] Determined from *S*-**19b**.

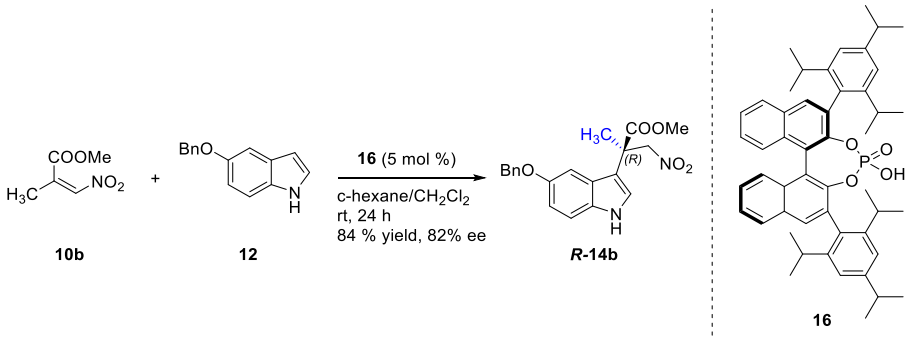

Scheme 2. Asymmetric Friedel–Craft reaction using chiral phosphoric acid. Reaction conditions: Nitroalkene 2 eq., 5-benzyloxyindole 1 eq., catalyst loading 5 mol % and MS5Å in cyclohexane/CH_2Cl_2 (v/v = 4:1). Enantiomeric excess was determined with chiral HPLC from *R*-**19b**.

inhibition assays could be transferred to potential biological activities, MV4-11 cells were treated with the compounds and the effect on HDAC6 inhibition was assessed by western blot [56]. As Marbostat-100 was studied in MV4-11 cells in the previous publication and the high relevance of HDAC6 in hematopoietic cells, this AML cell is ideal for further investigation of the synthesized compounds [29,56]. From a variety of cytosolic substrates, α-tubulin was chosen as a primary surrogate readout, since HDAC6 inhibition leads to increased tubulin acetylation [11]. To quantify tubulin acetylation, total protein was used as loading control in the western blots; HSP90 in Fig. 4 is only used for simplified presentation.

All tested compounds (**29a-f**) show a significant accumulation of hyperacetylated tubulin, although slight differences are observed depending on the residue at the chiral center. In contrast, hardly any band is visible in the DMSO control (Fig. 4A, B). The substitution at the indole (**29a** vs. **29f**) for a hydrogen has no impact on the hyperacetylation of tubulin. Overall, the western blot analyses confirm the K_i values determined from the *in vitro* HDAC inhibition assays.

To investigate any stereochemical effects in detail, **29b**, *S*-**29b**, and *R*-**29b** were compared to **4**, *S*-**4**, *R*-**4**, with Tubastatin A as a reference.

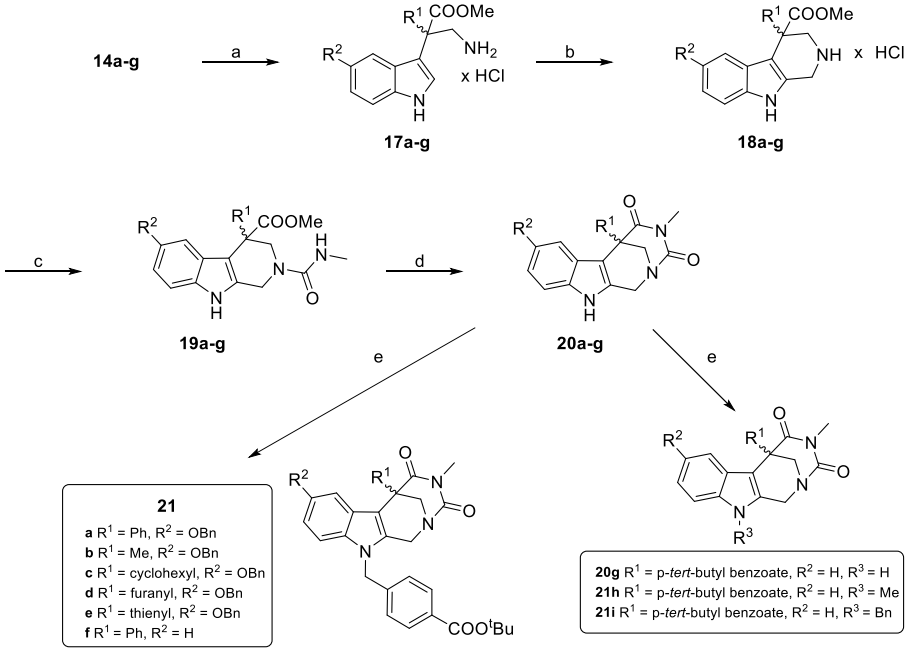

Scheme 3. Assembly the ring structure. Reagents and conditions a) zinc dust, $CuSO_4$, $HCl_{(aq)}$ (for **14g**: acetic acid), rt., 2 h, 79–99 %; b) formaldehyde (37 % in water), 60 °C,1 h, rt., 16 h, 58–99 %; c) DIPEA, 2,5-dioxopyrrolidin-1-yl-methylcarbamate, rt., 18 h, 53–99 %; d) Cs_2CO_3, argon, 115 °C, 1–3 d, 36–83 %; e) argon, NaH, 0 °C, 10 min, *tert*-butyl 4-(bromomethyl)benzoate or iodomethane or benzyl bromide, rt., 55–95 % 1–2 h.

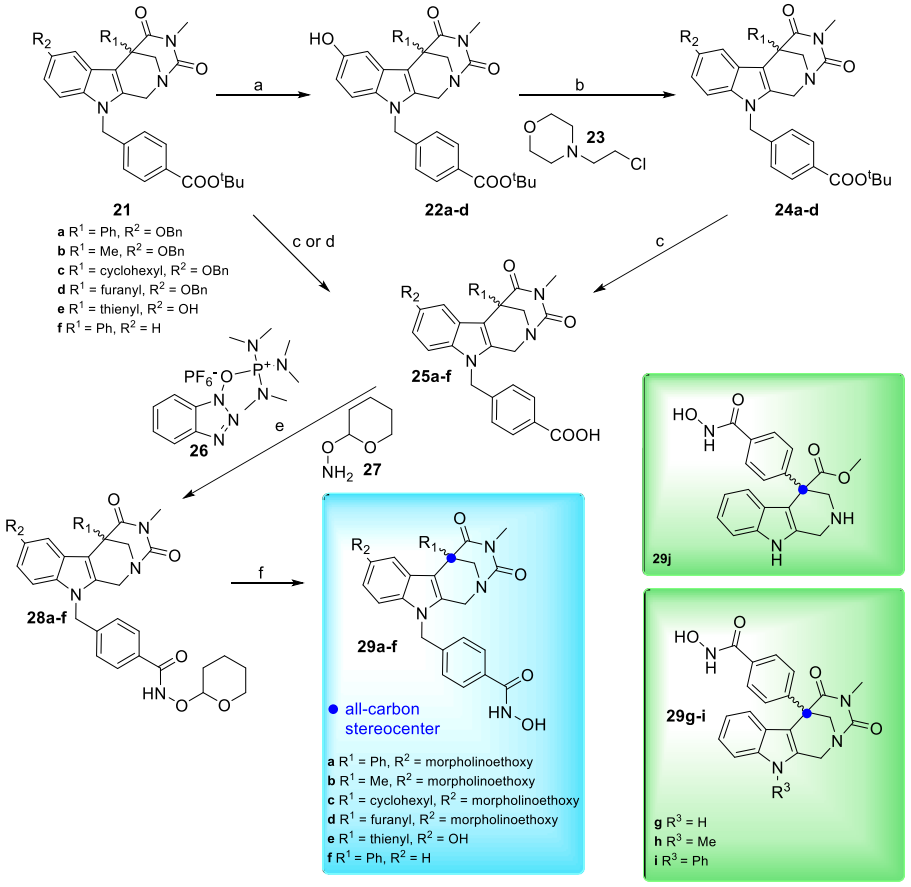

Scheme 4. Synthesis of the hydroxamic acid. a) H_2, Pd/C, rt., 2 h, 67–99 %; (b) Cs_2CO_3, 4-(2-chloroethyl)morpholine hydrochloride, 95 °C, 15 h, 52–92 %; (c) TFA, rt, 3 h, 91–99 %; (d) for **22d**: $BF_3{\cdot}OEt_2$, rt., 1 h, 88 %; (e) DMF, NEt_3, rt., 4 h, 54–99 %; (f) 6 M HCl in isopropanol, rt., 3 h, 58–88 %; synthesis of **29g-29j** follows the same approach and is shown in supporting information Scheme S1.

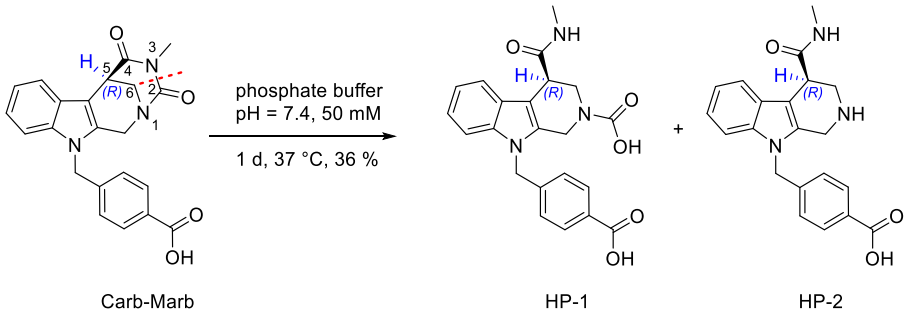

Fig. 2. Proposed point of hydrolysis (red dotted line) and decarboxylation at the dihydrouracil moiety. Precursor carboxylic acid of **4** (Carb-Marb) was incubated in phosphate buffer (50 mM, pH = 7.4) at 37 °C.

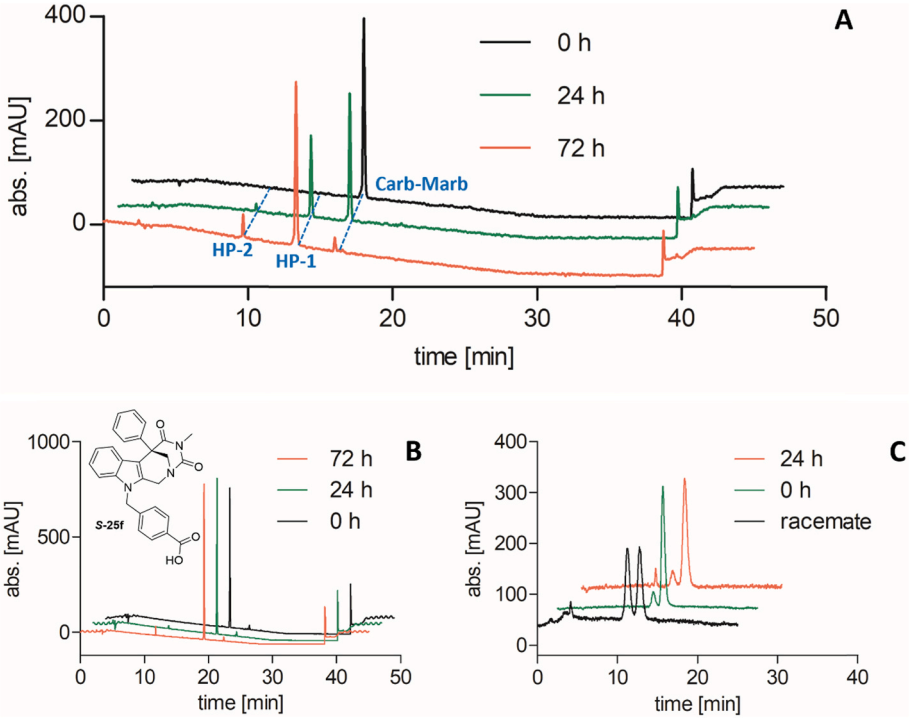

Fig. 3. HPLC traces of the Carb-Marb (**A**) and ***S*-25f** (**B**) after 0, 24 and 72 h incubation in phosphate buffer (pH = 7.4, 50 nM) at 37 °C. (**C**) Section of chiral HPLC traces of Carb-Marb after 0 and 24 h incubation in phosphate buffer (pH = 7.4, 50 nM) at 37 °C compared to the corresponding racemate.

Table 2
Stabilities of *S*-25b and *S*-29b in Human Plasma/PBS (1:2 v/v) (37 °C).

Compd.	24 h [a)]	72 h [a)]
***S*-25b**	91.4 ± 0.7	56.3 ± 1.0
***S*-29b**	83.9 ± 2.7	46.4 ± 2.3

[a)] % intact compound in plasma after the specified incubation times.

The racemates (**29**, **4**) exhibit a similar effect on the acetylation level. However, their configuration has a measurable influence on tubulin acetylation, with the (*S*)-enantiomers being superior to the (*R*)-enantiomers (Fig. 5).

To further highlight the improved ability of ***S*-29b** to cause alpha-tubulin hyperacetylation compared to Tubastatin A we extended the discussion of the data shown in Fig. 5 as follows: The kinetics of tubulin hyperacetylation were investigated by treating MV4-11 cells for different incubation times ranging from 20 min to 48 h. A pronounced accumulation of acetylated tubulin was observed just after 20 min. Within 13 h, hyperacetylation reached a plateau and did not decrease, even after incubation for 48 h (Fig. 4C, D). These results emphasize how rapidly and persistently ***S*-29b** interacts with the target enzyme, particularly in light of our previously published studies in which **4** showed a significant reduction in ac-tubulin in MV4-11 cells after 48 h [29]. The persistent effect can be explained by the superior stability of ***S*-29b** over **4** in the cell line.

Finally, we determined the effect of ***S*-29b** at different concentrations on the hyperacetylation. MV4-11 cells were treated with lower dose ranges from 5 nM to 500 nM (Fig. 4E, F) and higher dose ranges from 1 μM to 10 μM ***S*-29b** (Fig. 4G, H). At 5 nM a significant accumulation of ac-tubulin was observed. This effect peaked at 50 nM and hardly increased up to a concentration of 500 nM. In comparison, **4** did not cause hyperacetylation to the same extent at such low doses [29]. At higher doses, the increase in acetylated tubulin is less pronounced overall and decreases again from 6 μM. This is probably due to the degradation of the target enzyme, as a new band appears below it.

As we have previously demonstrated, hyperacetylation under **4** reached its peak at 16 h incubation time and decreased sharply until only a minimal effect was observed [29]. Since ***S*-29b** reaches its plateau at 13 h, with no descent even after 48 h (Fig. 4C, D), a more stable and longer lasting effect on the tubulin acetylation is to be expected.

Table 3
Influence of modifications at the chiral center on the *in vitro* HDAC inhibition assays against the HDAC subtypes HDAC1, HDAC2, HDAC3, HDAC6, and HDAC8.

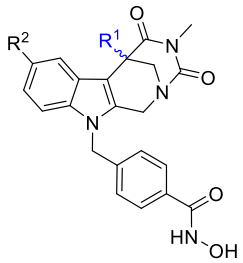

Compound Ki ± SD [nM]

entry	Compound ID	R^1 [a]	R^2	HDAC1[b]	HDAC2[c]	HDAC3[b]	HDAC6[c]	HDAC8[c]	HDAC10[c]
1[d]	**4**	H	H	358	774	306	0.7	173	ND
2	**29a**	Ph	morpholinoethoxy	227 ± 15	219 ± 32	510 ± 11	1.08 ± 0.51	843	ND
3	***S*-29a**	Ph (*S*)	morpholinoethoxy	136 ± 1.2	154 ± 24	315 ± 35	0.41 ± 0.20	1768	ND
4	**29f**	Ph	H	487 ± 89	514 ± 4	1174 ± 10	1.64 ± 0.81	ND	ND
5	***S*-29f**	Ph (*S*)	H	501 ± 52	263 ± 108	1177 ± 124	1.23 ± 0.56	ND	ND
6	**29b**	CH_3	morpholinoethoxy	132 ± 0.6	137 ± 22	279 ± 20	0.77 ± 0.57	762	ND
7	***S*-29b**	CH_3 (*S*)	morpholinoethoxy	60 ± 2.6	56 ± 9	162 ± 13	0.44 ± 0.33	362 ± 21	849 ± 98
8	***R*-29b**	CH_3 (*R*)	morpholinoethoxy	263 ± 27	519 ± 219	671 ± 137	1.08 ± 0.46	ND	ND
9	**29c**	c-hexyl	morpholinoethoxy	308 ± 47	323 ± 44	675 ± 93	1.25 ± 0.61	1094	ND
10	**29d**	furanyl	morpholinoethoxy	145 ± 19	120 ± 20	384 ± 19	0.44 ± 0.21	ND	ND
11	**29e**	thienyl	OH	103 ± 14[c]	260 ± 6	118 ± 4[c]	0.31 ± 0.04	ND	ND
12	**Tubastatin A**			1737 ± 99	1040	1957 ± 101	1.97	ND	ND
13	**Vorinostat**			41.0 ± 2.6	ND	33.8 ± 1.9	ND	ND	ND
14	**Trichostatin A**			0.26[c]	0.84 ± 0.49	0.14[c]	0.41 ± 0.03	438 ± 214	ND
15	**Quisinostat**			ND	ND	ND	ND	ND	1.49

[a] Racemic mixture unless stereoisomer indicated in brackets.
[b] Mean ± SD of at least two independent experiments, K_i was calculated from the respective IC_{50} values using the Cheng-Prusoff equation.
[c] Assays were performed by Reaction Biology Corporation. K_i was calculated from the respective IC_{50} values using the Cheng-Prusoff equation. ND: not determined.
[d] Data taken from reference [29].

Table 4
Influence of the linker moiety overturning on inhibition of HDAC6.

entry	Compound ID		R	Compound K_i [nM] HDAC6 [a]
1	**29g**	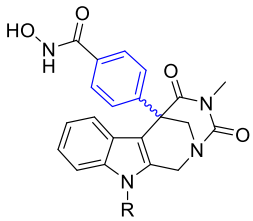	H	64
2	**29h**		CH_3	72
3	**29i**		Ph	247
4	**29j**	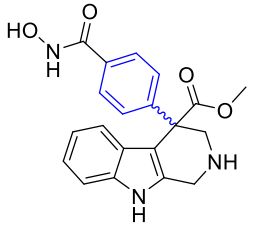		17

[a] Assays were performed by Reaction Biology Corporation. K_i was calculated from the respective IC_{50} values using the Cheng-Prusoff equation.

2.1. Antiproliferative activity

Compound *S*-**29b** was then evaluated for its antiproliferative activity against the leukemia cell lines MV4-11 using Tubastatin A and Ricolinostat as reference compounds. The results are summarized in Table 5. Compound *S*-**29b** (EC_{50} = 0.50 μM) showed strong antiproliferative activity and was 30-fold more active against MV4-11 cells than Tubastatin A (EC_{50} = 15.30 μM). Additionally, *S*-**29b** exceeded the activity of the clinical candidate Ricolinostat (EC_{50} = 0.71 μM). In conclusion, the selective HDAC6 inhibitor *S*-**29b** demonstrates substantial activity in cell viability assays, outperforming both Tubastatin A and Ricolinostat.

2.2. Structural characterization of the zHDAC6/S-29b complex

To better understand mechanistic underpinnings of the varied potency of our novel compounds (as observed in biochemical assays), we co-crystallized **29b** together with the second catalytic domains of zebrafish HDAC6 (zHDAC6-CD2). The complex crystallized in the $P2_12_12$ orthorhombic space group with a single molecule in the asymmetric unit and diffraction data were collected to the resolution limit of 1.59 Å (Table S2). Upon the structure solution using molecular replacement with the HDAC6/Tubastatin A structure as a starting model (PDB code 6THV) [37], the interpretable *Fo-Fc* difference electron density map representing the active site-bound inhibitor allowed for the unambiguous fitting of the compound in the final stages of the refinement (Fig. 6A). Interestingly, while crystallization droplets comprised a racemic mixture of *(R)* and *(S)*-enantiomers (**29b**), only the more potent *(S)*-enantiomer (*S*-**29b**) was observed in the final refined model.

The *S*-**29b** hydroxamate moiety coordinates the active-site zinc ion in a bidentate fashion with interatomic distances of 2.05 and 2.26 Å for the N-OH and C=O group, respectively (Fig. 6B). The hydroxamate carbonyl group is further hydrogen bonded to the Y745 hydroxyl group (2.4 Å), D705 carboxylate (2.9 Å), and H614 amine (3.1 Å) and the N-OH function forms a network of H-bonds with side chains of H573 (2.6 Å), H574 (2.8 and 3.1 Å), D612 (2.9 Å), and H614 (2.7 and 3.1 Å). The phenyl ring of the linker is placed between the side chains of F583 and F643 with distances of 3.8 Å and 5.0 Å between the respective ring centers (Fig. 6D). The indole moiety of the capping group does not make any direct hydrogen bond interactions with protein residues, but it is in a close contact with a hydrophobic patch delineated by amino acids of the

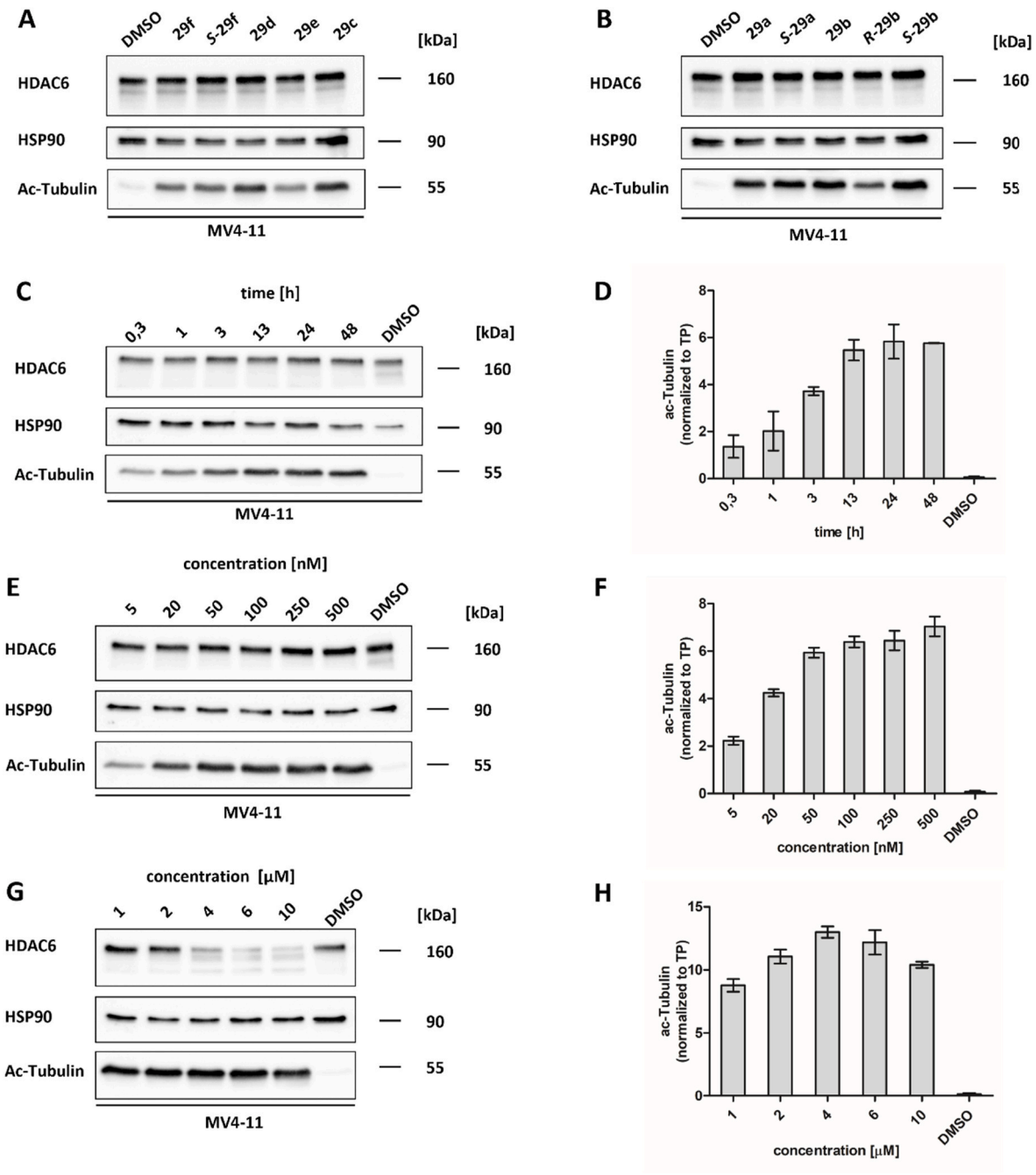

Fig. 4. Immunoblot analysis of synthesized compounds. (A)/(B) MV4-11 cells were treated with 100 nM of compounds **29a-f** for 24 h. (C) MV4-11 cells were treated with 50 nM ***S***-29b for 0.3, 1, 3, 13, 24 and 48 h. (D) Densitometry analysis of ac-Tubulin/Total Protein [%]. (E) MV4-11 cells were treated with 5, 20, 50, 100, 250 and 500 nM ***S***-29b for 24 h. (F) Densitometry analysis of ac-Tubulin/Total Protein [%]. (G) MV4-11 cells were treated with 1, 2, 4, 6 and 10 µM ***S***-29b for 24 h. (H) Densitometry analysis of ac-Tubulin/Total Protein [%]. MV4-11 cells were analyzed by Western blot assay to compare the effect on tubulin acetylation. Total Protein was used as loading control for the qualitative evaluation, HSP90 is only used for simplified visualization. Negative control with DMSO. One representative western blot of at least two independent experiments is shown. Bar diagram showing cellular ac-Tubulin normalized to Total Protein [%] level upon degrader treatment. Bars represent mean ± SD of n = 2 biological replicates.

L1-loop pocket – side chains of H463, P464, F583, and L712 (Fig. 6C). The C5 carbon of the ***S*-29b** indole ring is functionalized by the morpholinoethoxy moiety. Contrary to the remaining of the ***S*-29b** inhibitor, the *Fo-Fc* electron density peaks of the morpholinoethoxy group are quite weak pointing towards its positional flexibility (Fig. 6A) and the absence of interactions with the enzyme.

The dihydrouracil moiety of the inhibitor extends towards the L2 loop (amino acids G640 – N645) [37], where the N3 capping methyl group and one of the ring carbons make van der Waals contacts with benzyl moieties of F642 (4.3 Å) and F643 (4.0 Å), respectively, and the C_2 carbonyl oxygen forms a hydrogen bond with the His614 side chain (2.8 Å; Fig. 6D). Finally, the methyl moiety at the all-carbon stereocenter is oriented towards the bulk solution away from the protein surface and does not thus contribute to inhibitor/enzyme interactions. This observation is in line with inhibition data where substitutions at the all-carbon stereocenter do not change inhibitor potency for HDAC6. At the same time, however, changing stereochemistry at the all-carbon stereocenter would disturb observed interactions pattern with the

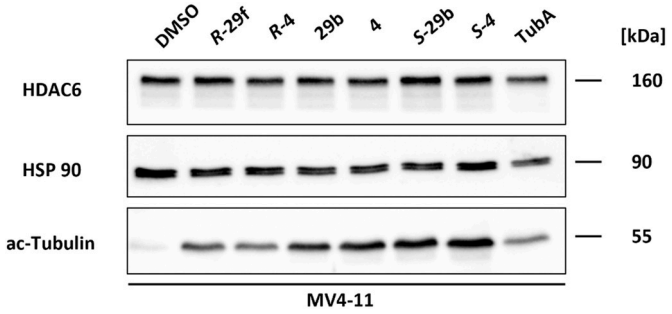

Fig. 5. Immunoblot analysis of Marbostat-100 (**4**), **29b** and the corresponding *S*- and *R*-enantiomers and Tubastatin A (TubA). MV4-11 cells were treated with 100 nM of compounds for 24 h. Negative control with DMSO.

Table 5
Antiproliferative activities of *S*-**29b**, Tubastatin A, and Ricolinostat in MV4-11 cells.[a]

Compound ID	EC_{50}
***S*-29b**	0.50 ± 0.14
Tubastatin A	15.30 ± 1.17
Ricolinostat	0.71 ± 0.12

[a] CellTiter-Glo luminescent cell viability assay upon a 72 h treatment of MV4-11 cells with the respective compound. Data represents mean ± SD of three independent biological experiments.

(R)-enantiomers being less favored related to their *(S)* counterparts.

When zHDAC6/*S*-**29b** and zHDAC6/Tubastatin A complexed are superimposed (Fig. 7A), several differences exist in the positioning of the two compounds. Most importantly, while a bidentate coordination of the active-site Zn^{2+} ion is observed for *S*-**29b**, the hydroxamate group of Tubastatin A coordinates the ion in a monodentate fashion via its negatively charged N-O^- group. Differences in Zn^{2+} coordination are then manifested in the positional shift of the phenylalanine linker that is pulled by 0.45 Å towards the active-site Zn^{2+} ion (Fig. 7B). Finally, the capping groups are rotated by approximately 13° within the plane of the indole ring (Fig. 7C) of each other and the rotation can be in part elicited *via* additional attractive interactions between the dihydrouracil moiety of *S*-**29b** and HDAC6 residues.

3. Conclusion

Using a Friedel-Crafts reaction, we were able to substitute the acidic hydrogen of **4** with a range of carbon residues to generate an all-carbon quaternary stereocenter. In addition to the racemates, the corresponding

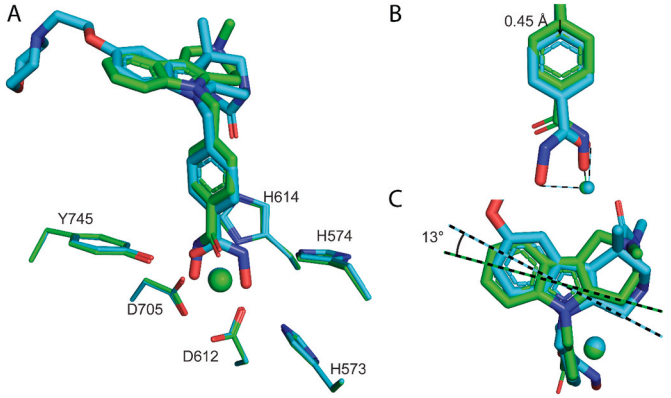

Fig. 7. Superposition of zHDAC6 complexes with Tubastatin A (carbons and the Zn ions colored green) and *S*-**29b** (carbons and the Zn ions colored cyan). **Panel A**: an overall view of superposed residues in the vicinity of the active-site Zn^{2+}. **Panel B**: Differences in Zn^{2+} coordination between TubA (monodentate) and *S*-**29b** (bidentate) are associated with the shift of the phenylalanine linker by 0.45 A. **Panel C**: Rotation of the cap groups of TubA and *S*-**29b** by 13°.

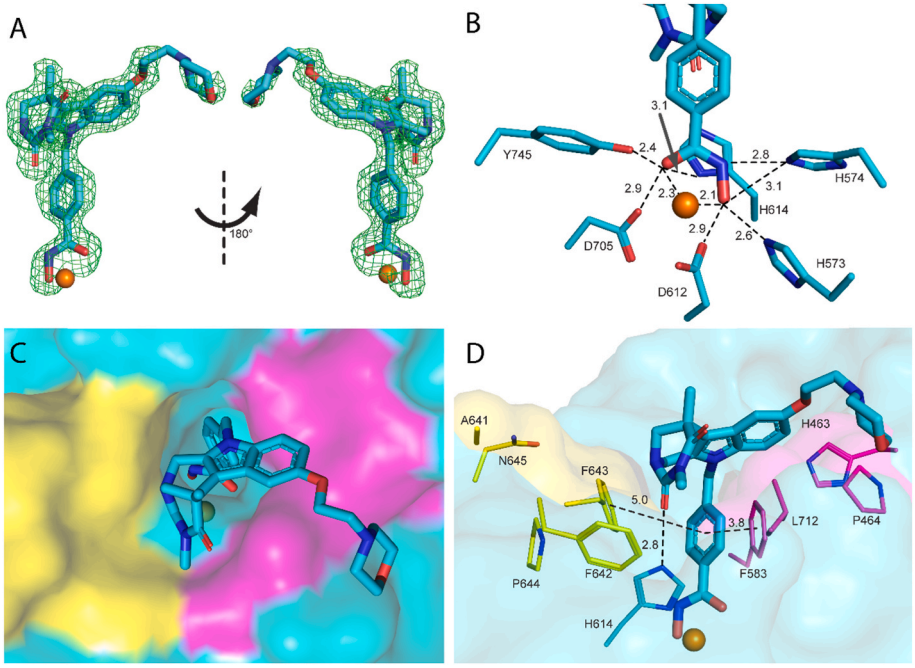

Fig. 6. Crystal structure of the zHDAC6/*S*-**29b** complex. **Panel A**: The *Fo-Fc* omit map (green) is contoured at 3.0 σ and the inhibitor is shown in stick representation with atoms colored red (oxygen), blue (nitrogen), and cyan (carbon). The active-site zinc ion is shown as an orange sphere. **Panel B**: Interactions pattern of the *S*-**29b** hydroxamate moiety (stick representation) in the active site of zHD6 (line representation). **Panels C**, **D**: The L1-loop pocket (formed by side chains of H463, P464, F583, and L712) and the L2-loop pocket (amino acids G640 – N645) are colored purple and yellow, respectively. The surface of zHDAC6 is shown in a (semi-transparent) surface representation. Distances are shown in Ångstroms (dashed lines).

enantiomers were also accessible via various catalysts. The introduction of the carbon residue has a positive effect on the hydrolytic stability of the inhibitors dihydrouracil moiety. Data derived from *in vitro* HDAC inhibition assays demonstrate that derivatives **29a-f** are highly selective and potent inhibitors of HDAC6. Incubation of MV4-11 with the compounds resulted in a strong tubulin hyperacetylation caused by HDAC6 inhibition. Overall, derivatization at the stereocenter did not impact the potency of the inhibitor. However, the stereochemistry and orientation of the dihydrouracil moiety influences inhibition of HDAC6, favoring (S)-configurated **29a**,**b**,**f**. These observations were confirmed by a zHDAC6-CD2 crystal complex with *S*-**29b**. Further investigations in the cell-based assay showed that *S*-**29b** causes tubulin acetylation at lower doses than **4** and has a longer-lasting effect.

Funding

This work was in part supported by the Czech Academy of Sciences (RVO: 86652036) and the Ministry of Education, Youth and Sports (MEYS - LUAUS23247). We acknowledge CMS-Biocev (Biophysical techniques, crystallization, and structural MS), Instruct-CZ Centre, supported by MEYS CR (LM2018127) and the Helmholtz-Zentrum Berlin for the allocation of synchrotron radiation beamtime at the MX14.2 beamline (project CALIPSOplus, grant agreement 730872).

Dedicated to the 92nd birthday of Professor Dr. Dr. Wolfgang Wiegrebe.

CRediT authorship contribution statement

Simon Scheuerer: Writing – original draft, Visualization, Validation, Project administration, Investigation. **Lucia Motlova:** Writing – original draft, Validation, Investigation. **Linda Schäker-Hübner:** Writing – review & editing, Writing – original draft, Visualization, Validation, Investigation. **Andreas Sellmer:** Writing – review & editing. **Felix Feller:** Investigation. **Fabian J. Ertl:** Investigation. **Pierre Koch:** Supervision. **Finn K. Hansen:** Writing – review & editing, Supervision. **Cyril Barinka:** Writing – review & editing, Supervision. **Siavosh Mahboobi:** Writing – review & editing, Supervision, Project administration, Conceptualization.

Declaration of competing interest

The authors declare that they have no known competing financial interests or personal relationships that could have appeared to influence the work reported in this paper.

Data availability

No data was used for the research described in the article.

Appendix A. Supplementary data

Supplementary data to this article can be found online at https://doi.org/10.1016/j.ejmech.2024.116676.

References

[1] T. Jenuwein, C.D. Allis, Translating the histone code, Science 293 (2001) 1074–1080.
[2] E. Seto, M. Yoshida, Erasers of histone acetylation: the histone deacetylase enzymes, Cold Spring Harbor Perspect. Biol. 6 (2014) a018713.
[3] A. Inoue, D. Fujimoto, Enzymatic deacetylation of histone, Biochem. Biophys. Res. Commun. 36 (1969) 146–150.
[4] T. Kouzarides, Chromatin modifications and their function, Cell 128 (2007) 693–705.
[5] Y. Li, D. Shin, S.H. Kwon, Histone deacetylase 6 plays a role as a distinct regulator of diverse cellular processes, FEBS J. 280 (2013) 775–793.
[6] M. Ocker, Deacetylase inhibitors - focus on non-histone targets and effects, World J. Biol. Chem. 1 (2010) 55–61.
[7] P.A. Marks, Histone deacetylase inhibitors: a chemical genetics approach to understanding cellular functions, Biochim. Biophys. Acta 1799 (2010) 717–725.
[8] M. Yoshida, R. Furumai, M. Nishiyama, Y. Komatsu, N. Nishino, S. Horinouchi, Histone deacetylase as a new target for cancer chemotherapy, Cancer Chemother. Pharmacol. 48 (Suppl 1) (2001) S20–S26.
[9] X.-H. Zhang, Qin-Ma, H.-P. Wu, M.Y. Khamis, Y.-H. Li, L.-Y. Ma, H.-M. Liu, A review of progress in histone deacetylase 6 inhibitors research: structural specificity and functional diversity, J. Med. Chem. 64 (2021) 1362–1391.
[10] Y. Hai, D.W. Christianson, Histone deacetylase 6 structure and molecular basis of catalysis and inhibition, Nat. Chem. Biol. 12 (2016) 741–747.
[11] Y. Zhang, N. Li, C. Caron, G. Matthias, D. Hess, S. Khochbin, P. Matthias, HDAC-6 interacts with and deacetylates tubulin and microtubules in vivo, EMBO J. 22 (2003) 1168–1179.
[12] C. Hubbert, A. Guardiola, R. Shao, Y. Kawaguchi, A. Ito, A. Nixon, M. Yoshida, X.-F. Wang, T.-P. Yao, HDAC6 is a microtubule-associated deacetylase, Nature 417 (2002) 455–458.
[13] J.J. Kovacs, P.J.M. Murphy, S. Gaillard, X. Zhao, J.-T. Wu, C.V. Nicchitta, M. Yoshida, D.O. Toft, W.B. Pratt, T.-P. Yao, HDAC6 regulates Hsp90 acetylation and chaperone-dependent activation of glucocorticoid receptor, Mol. Cell 18 (2005) 601–607.
[14] X. Zhang, Z. Yuan, Y. Zhang, S. Yong, A. Salas-Burgos, J. Koomen, N. Olashaw, J. T. Parsons, X.-J. Yang, S.R. Dent, T.-P. Yao, W.S. Lane, E. Seto, HDAC6 modulates cell motility by altering the acetylation level of cortactin, Mol. Cell 27 (2007) 197–213.
[15] R.B. Parmigiani, W.S. Xu, G. Venta-Perez, H. Erdjument-Bromage, M. Yaneva, P. Tempst, P.A. Marks, HDAC6 is a specific deacetylase of peroxiredoxins and is involved in redox regulation, Proc. Natl. Acad. Sci. U.S.A. 105 (2008) 9633–9638.
[16] S. Zhao, W. Xu, W. Jiang, W. Yu, Y. Lin, T. Zhang, J. Yao, L. Zhou, Y. Zeng, H. Li, Y. Li, J. Shi, W. An, S.M. Hancock, F. He, L. Qin, J. Chin, P. Yang, X. Chen, Q. Lei, Y. Xiong, K.-L. Guan, Regulation of cellular metabolism by protein lysine acetylation, Science 327 (2010) 1000–1004.
[17] T. Li, C. Zhang, S. Hassan, X. Liu, F. Song, K. Chen, W. Zhang, J. Yang, Histone deacetylase 6 in cancer, J. Hematol. Oncol. 11 (2018) 111.
[18] C. Simões-Pires, V. Zwick, A. Nurisso, E. Schenker, P.-A. Carrupt, M. Cuendet, HDAC6 as a target for neurodegenerative diseases: what makes it different from the other HDACs? Mol. Neurodegener. 8 (2013) 7.
[19] J. Iaconelli, J.H. Huang, S.S. Berkovitch, S. Chattopadhyay, R. Mazitschek, S. L. Schreiber, S.J. Haggarty, R. Karmacharya, HDAC6 inhibitors modulate Lys49 acetylation and membrane localization of β-catenin in human iPSC-derived neuronal cells, ACS Chem. Biol. 10 (2015) 883–890.
[20] C. Seidel, M. Schnekenburger, M. Dicato, M. Diederich, Histone deacetylase 6 in health and disease, Epigenomics 7 (2015) 103–118.
[21] T.C.S. Ho, A.H.Y. Chan, A. Ganesan, Thirty years of HDAC inhibitors: 2020 insight and hindsight, J. Med. Chem. 63 (2020) 12460–12484.
[22] D.J. DeAngelo, R.A. Mesa, W. Fiskus, A. Tefferi, C. Paley, M. Wadleigh, E. K. Ritchie, D.S. Snyder, K. Begna, S. Ganguly, M.S. Ondovik, J. Rine, K.N. Bhalla, Phase II trial of panobinostat, an oral pan-deacetylase inhibitor in patients with primary myelofibrosis, post-essential thrombocythaemia, and post-polycythaemia vera myelofibrosis, Br. J. Haematol. 162 (2013) 326–335.
[23] M. Duvic, R. Talpur, X. Ni, C. Zhang, P. Hazarika, C. Kelly, J.H. Chiao, J.F. Reilly, J. L. Ricker, V.M. Richon, S.R. Frankel, Phase 2 trial of oral vorinostat (suberoylanilide hydroxamic acid, SAHA) for refractory cutaneous T-cell lymphoma (CTCL), Blood 109 (2007) 31–39.
[24] R.L. Piekarz, R. Frye, M. Turner, J.J. Wright, S.L. Allen, M.H. Kirschbaum, J. Zain, H.M. Prince, J.P. Leonard, L.J. Geskin, C. Reeder, D. Joske, W.D. Figg, E. R. Gardner, S.M. Steinberg, E.S. Jaffe, M. Stetler-Stevenson, S. Lade, A.T. Fojo, S. E. Bates, Phase II multi-institutional trial of the histone deacetylase inhibitor romidepsin as monotherapy for patients with cutaneous T-cell lymphoma, J. Clin. Oncol. 27 (2009) 5410–5417.
[25] M. Cosenza, S. Pozzi, The therapeutic strategy of HDAC6 inhibitors in lymphoproliferative disease, Int. J. Mol. Sci. 19 (2018).
[26] Y. Zhang, S. Kwon, T. Yamaguchi, F. Cubizolles, S. Rousseaux, M. Kneissel, C. Cao, N. Li, H.-L. Cheng, K. Chua, D. Lombard, A. Mizeracki, G. Matthias, F.W. Alt, S. Khochbin, P. Matthias, Mice lacking histone deacetylase 6 have hyperacetylated tubulin but are viable and develop normally, Mol. Cell Biol. 28 (2008) 1688–1701.
[27] D.T. Vogl, N. Raje, S. Jagannath, P. Richardson, P. Hari, R. Orlowski, J.G. Supko, D. Tamang, M. Yang, S.S. Jones, C. Wheeler, R.J. Markelewicz, S. Lonial, Ricolinostat, the first selective histone deacetylase 6 inhibitor, in combination with bortezomib and dexamethasone for relapsed or refractory multiple myeloma, Clin. Cancer Res. 23 (2017) 3307–3315.
[28] E. Pontiki, D. Hadjipavlou-Litina, Histone deacetylase inhibitors (HDACIs). Structure–activity relationships: history and new QSAR perspectives, Med. Res. Rev. 32 (2012) 1–165.
[29] A. Sellmer, H. Stangl, M. Beyer, E. Grünstein, M. Leonhardt, H. Pongratz, E. Eichhorn, S. Elz, B. Striegl, Z. Jenei-Lanzl, S. Dove, R.H. Straub, O.H. Krämer, S. Mahboobi, Marbostat-100 defines a new class of potent and selective antiinflammatory and antirheumatic histone deacetylase 6 inhibitors, J. Med. Chem. 61 (2018) 3454–3477.
[30] S. Shen, A.P. Kozikowski, Why hydroxamates may not Be the best histone deacetylase inhibitors–what some may have forgotten or would rather forget? ChemMedChem 11 (2016) 15–21.
[31] Faridoon, Y.L. Zha, G. Zhang, J.J. Li, Medicinal chemistry insights into non-hydroxamate HDAC6 selective inhibitors, Med. Chem. Res. 32 (2023) 1–14.
[32] K. Yue, S. Sun, G. Jia, M. Qin, X. Hou, C.J. Chou, C. Huang, X. Li, First-in-Class hydrazide-based HDAC6 selective inhibitor with potent oral anti-inflammatory

activity by attenuating NLRP3 inflammasome activation, J. Med. Chem. 65 (2022) 12140–12162.
[33] E. Cellupica, G. Caprini, P. Cordella, C. Cukier, G. Fossati, M. Marchini, I. Rocchio, G. Sandrone, M.A. Vanoni, B. Vergani, K. Źrubek, A. Stevenazzi, C. Steinkühler, Difluoromethyl-1,3,4-oxadiazoles are slow-binding substrate analog inhibitors of histone deacetylase 6 with unprecedented isotype selectivity, J. Biol. Chem. (2022) 102800.
[34] B. König, P.R. Watson, N. Reßing, A.D. Cragin, L. Schäker-Hübner, D. W. Christianson, F.K. Hansen, Difluoromethyl-1,3,4-oxadiazoles are selective, mechanism-based, and essentially irreversible inhibitors of histone deacetylase 6, J. Med. Chem. 66 (2023) 13821–13837.
[35] L. Motlová, I. Šnajdr, Z. Kutil, E. Andris, J. Ptáček, A. Novotná, Z. Nováková, B. Havlínová, W. Tueckmantel, H. Dráberová, P. Majer, M. Schutkowski, A. Kozikowski, L. Rulíšek, C. Bařinka, Comprehensive mechanistic view of the hydrolysis of oxadiazole-based inhibitors by histone deacetylase 6 (HDAC6), ACS Chem. Biol. 18 (2023) 1594–1610.
[36] K.V. Butler, J. Kalin, C. Brochier, G. Vistoli, B. Langley, A.P. Kozikowski, Rational design and simple chemistry yield a superior, neuroprotective HDAC6 inhibitor, tubastatin A, J. Am. Chem. Soc. 132 (2010) 10842–10846.
[37] S. Shen, M. Svoboda, G. Zhang, M.A. Cavasin, L. Motlova, T.A. McKinsey, J. H. Eubanks, C. Bařinka, A.P. Kozikowski, Structural and in vivo characterization of tubastatin A, a widely used histone deacetylase 6 inhibitor, ACS Med. Chem. Lett. 11 (2020) 706–712.
[38] M. Feofanov, M. Anokhin, A. Averin, I. Beletskaya, The friedel–crafts reaction of indoles with Michael acceptors catalyzed by magnesium and calcium salts, Synthesis 49 (2017) 5045–5058.
[39] J.-Q. Weng, Q.-M. Deng, L. Wu, K. Xu, H. Wu, R.-R. Liu, J.-R. Gao, Y.-X. Jia, Asymmetric Friedel-Crafts alkylation of α-substituted β-nitroacrylates: access to β(2,2)-amino acids bearing indolic all-carbon quaternary stereocenters, Org. Lett. 16 (2014) 776–779.
[40] W. Xu, X. Shen, Q. Ma, L. Gong, E. Meggers, Restricted conformation of a hydrogen bond mediated catalyst enables the highly efficient enantioselective construction of an all-carbon quaternary stereocenter, ACS Catal. 6 (2016) 7641–7646.
[41] K. Mori, M. Wakazawa, T. Akiyama, Stereoselective construction of all-carbon quaternary center by means of chiral phosphoric acid: highly enantioselective Friedel–Crafts reaction of indoles with β,β-disubstituted nitroalkenes, Chem. Sci. 5 (2014) 1799–1803.
[42] W. Xu, M. Arieno, H. Löw, K. Huang, X. Xie, T. Cruchter, Q. Ma, J. Xi, B. Huang, O. Wiest, L. Gong, E. Meggers, Metal-templated design: enantioselective hydrogen-bond-driven catalysis requiring only parts-per-million catalyst loading, J. Am. Chem. Soc. 138 (2016) 8774–8780.
[43] R.A. Lazarus, Chemical racemization of 5-benzylhydantoin, J. Org. Chem. 55 (1990) 4755–4757.
[44] I.B. Blagoeva, I.G. Pojarlieff, V.S. Dimitrov, Alkaline hydrolysis of hydantoin, 3-methylhydantoin, and 1-acetyl-3-methylurea. Effect of ring size on the cleavage of acylureas, J. Chem. Soc., Perkin Trans. 2 (1978) 887.
[45] A. Ballard, H.O. Ahmad, S. Narduolo, L. Rosa, N. Chand, D.A. Cosgrove, P. Varkonyi, N. Asaad, S. Tomasi, N.J. Buurma, A.G. Leach, Quantitative prediction of rate constants for aqueous racemization to avoid pointless stereoselective syntheses, Angew. Chem. 130 (2018) 994–997.
[46] A.-C. Cabordery, M. Toussaint, N. Azaroual, J.-P. Bonte, P. Melnyk, C. Vaccher, C. Foulon, Kinetics and mechanism of racemization of Tic-hydantoins, potent sigma-1 agonists, Tetrahedron: Asymmetry 22 (2011) 125–133.
[47] B. Knoche, G. Blaschke, Investigations on the in vitro racemization of thalidomide by high-performance liquid chromatography, J. Chromatogr. A 666 (1994) 235–240.
[48] C. Pepper, H.J. Smith, K.J. Barrell, P.J. Nicholls, M.J. Hewlins, Racemisation of drug enantiomers by benzylic proton abstraction at physiological pH, Chirality 6 (1994) 400–404.
[49] K.H. Dudley, D.L. Bius, Buffer catalysis of the racemization reaction of some 5-phenylhydantoins and its relation to the in vivo metabolism of ethotoin, Drug Metab. Dispos. 4 (1976) 340–348.
[50] H. Tomizawa, H. Yamada, K. Wada, T. Imoto, Stabilization of lysozyme against irreversible inactivation by suppression of chemical reactions, J. Biochem. 117 (1995) 635–640.
[51] A. Argyrou, M.W. Washabaugh, Proton transfer from the C 5 - proR/proS positions of l -dihydroorotate: general-base catalysis, isotope effects, and internal return 1, J. Am. Chem. Soc. 121 (1999) 12054–12062.
[52] A.I. Martínez-Gómez, J.M. Clemente-Jiménez, F. Rodríguez-Vico, L.T. Kanerva, X.-G. Li, F.J.L. Heras-Vázquez, S. Martínez-Rodríguez, New biocatalytic route for the production of enantioenriched β-alanine derivatives starting from 5- and 6-mono-substituted dihydrouracils, Process Biochem. 47 (2012) 2090–2096.
[53] K. Nishimura, Y. Hashimoto, S. Iwasaki, (S)-form of alpha-methyl-N(alpha)-phthalimidoglutarimide, but not its (R)-form, enhanced phorbol ester-induced tumor necrosis factor-alpha production by human leukemia cell HL-60: implication of optical resolution of thalidomidal effects, Chem. Pharm. Bull. 42 (1994) 1157–1159.
[54] E. Tokunaga, T. Yamamoto, E. Ito, N. Shibata, Understanding the thalidomide chirality in biological processes by the self-disproportionation of enantiomers, Sci. Rep. 8 (2018) 17131.
[55] M. Reist, P.-A. Carrupt, B. Testa, S. Lehmann, J.J. Hansen, Kinetics and mechanisms of racemization: 5-substituted hydantoins (= imidazolidine-2,4-diones) as models of chiral drugs, Helv. Chim. Acta 79 (1996) 767–778.
[56] O.H. Krämer, S. Mahboobi, A. Sellmer, Drugging the HDAC6-HSP90 interplay in malignant cells, Trends Pharmacol. Sci. 35 (2014) 501–509.